

**TOURMALINES FROM THE STEWART MINE, PALA, SAN DIEGO COUNTY,  
CALIFORNIA: CHEMISTRY AND CRYSTAL STRUCTURE**

JOHN M. HUGHES<sup>1</sup> AND JACOB MENKEN

*Department of Geology, The University of Vermont, Burlington, VT 05405, U.S.A.*

ANDREAS ERTL

*Institut für Mineralogie und Kristallographie, Geozentrum, Universität Wien,  
Althanstrasse 14, 1090 Wien, Austria*

ABSTRACT

*Keywords:* tourmaline, crystal structure, Stewart mine, distortion

SOMMAIRE

*Mots-clés:*

*Keywords:* tourmaline, crystal structure, Stewart mine

---

<sup>1</sup> *E-mail address:* [jmhughes@uvm.edu](mailto:jmhughes@uvm.edu)

## INTRODUCTION

The tourmaline group minerals are aluminoborocyclosilicates typically found in late-stage igneous rocks. In the past decade, extensive study has been undertaken on the tourmaline atomic arrangement (Bosi *et al.* 2007, Hawthorne 2002, Novák *et al.* 2011, Van Hinsberg *et al.* 2011). Those studies have elucidated the extensive substitution in the cation sites in the tourmaline atomic arrangement and the range of chemical composition among tourmalines, and also revised the nomenclature of the tourmaline minerals (Hawthorne *et al.* 1999).

The Pala Mining District located in Pala, San Diego County, California is home to some of the world's greatest deposits of gem-quality tourmaline. While formal mining operations in the Pala Mining District began in the 1870's, the Stewart mine first began producing lepidolite in 1892. Tourmaline gems from the Stewart mine were mined in the middle 1930s. In addition to tourmaline mining, the Pala Mining District is home to several large mining operations including various lithium and feldspar mines as well as other gem mineral mines including quartz and spodumene. (Jahns *et al.* 1951). The Tourmaline Queen mine and the Himalaya mine are also located in San Diego County, California. The tourmaline from Himalaya mine has been extensively studied (Ertl *et al.* 2010).

## GEOLOGIC SETTING

The gem-bearing pegmatite dikes of the San Diego County region of Southern California are intruded into Cretaceous-age Peninsular Ranges Batholith, also known as the Southern California Batholith. Granitic pegmatitic-aplite dikes found in San Diego County and the Stewart mine region can be found as dike swarms or as individual units.

The dikes found in this region are primarily found in older gabbros and tonalities found in the Southern California Batholith, however, dikes from complex can be found in even older, pre-Southern California Batholith, metasedimentary units (Taylor *et al.* 1979).

Lepidolite from the Stewart mine was dated at approximately 110 m.y. using Rb/Sr dating methods by Herzog *et al.* (1960). The Stewart mine pegmatite dikes were emplaced at temperatures of 700-730°C and pressures of 2.1-2.2 kb (London 1986). The gem-bearing inclusions from the pegmatite-aplite dikes of the San Diego County and Stewart mine region originated from an aqueous fluid at a temperature of 520-525°C and at a pressure of 2.0 kb (Taylor *et al.* 1979). Values of the pressure of emplacement were also reported by Taylor *et al.*, who found emplacement pressures between 2.1-2.2 kb. Assuming an emplacement pressure of 2.1-2.2 kb, the pegmatite dikes were emplaced at a depth of 6.8-7.6 km (Taylor *et al.* 1979).

## EXPERIMENTAL DETAILS

### *Crystal Structure*

Tourmaline crystals ~50µm in size were mounted onto a Bruker APEX II diffractometer equipped with a graphite-monochromatized MoK $\alpha$ . Scan times varied from 7.5 to 14.0 seconds per frame. Refined cell parameters and other crystallographic information are included in Table 1.

Redundant data were collected for a sphere of reciprocal space and were integrated and corrected for Lorentz and polarization factors. The structure was refined using a tourmaline starting model and full-matrix least-squares on F<sup>2</sup> in SHELXL-97 (Sheldrick 2008).

The *B*, *Z*(=Al), O1-O8 and H3 sites were constrained to full-occupancy at their respective bonding site. The *Y* site was modeled as being occupied by Li, Al, Fe and/or Mg. The *T* site was modeled with the Si and B scattering factors such that  $Si+B=1$ .

Structure factors can be obtained from the Depository of Unpublished data, CISTI, National Research Council, Ottawa, Ontario K1A 0S2, Canada. Table 2 provides the atomic parameters for the samples analyzed, bond valence sums and Table 3 displays the interatomic distances of the samples analyzed.

### *Tourmaline Chemistry*

Electron probe microanalysis (EMPA) was used to analyze all elements detected except H, Li, Be and B. EMPA data was obtained using a CAMECA SX51 electron microprobe (EPMA) equipped with wavelength-dispersive spectrometers located at Universität Heidelberg in Germany. Concentrations of the light elements H, Li, Be and B were obtained using a secondary ion mass spectrometer (SIMS) with a CAMECA ims 3f ion microprobe also located at Universität Heidelberg.

## RESULTS AND DISCUSSION

### *SIMS and EMPA analysis*

The results of SIMS and EPMA chemical analysis of the samples are displayed in the Table 4. Tourmaline formulas were calculated on the basis of 31 oxygens per formula unit and are displayed on Table 5. Due to Si not totally filling the *T* site, in samples STEWCL, STEWMP, STEWLG, STEWCO and STEWMG, the *T* site vacancies were filled with B; this substitution is validated by the  $\langle T-O \rangle$  bond-distance range between

1.616-1.617Å, less than the putative 1.62Å distance in tourmaline structures. Samples STEWMC and STEWS *T* sites were either fully occupied by Si or contained small amounts of Al due to <*T*-O> bond-distances varying between 1.620 - 1.621Å. OH+F was calculated  $OH + F - (O = F) = 4.0$ . SIMS and EMPA analysis yielded an overabundance of Al *apfu* (atoms per formula unit) thus the *Z* site was occupied by Al = 6.0 before any Al was distributed to the *Y* or *T* sites. *X* site occupancies included Ca, Na and vacancies. *Y* sites were occupied by Mg, Fe and Li as well as Mn, Zn and Ti, *Z* sites were completely occupied by Al.

The differences in concentration of Li in the samples analyzed could be caused by increasing magmatic differentiation. Pegmatitic rock bodies typically display increased Li concentrations with increased magmatic differentiation (Marschal *et al.* 2011). Thus, sample STEWS is the least differentiated sample due to it having the lowest Li *apfu* content analyzed at 0.04. Conversely, sample STEWMC is the most differentiated due to it having the highest Li *apfu* content analyzed at 0.96. STEWMC and STEWS are the two samples that both contain Al at the *T* site and respectively have the most and least Li.

### *Crystal Structure*

The full structural formulas for the tourmaline samples from the Stewart Mine are displayed in Table 5. The tourmaline samples found at the Stewart mine are most comprised elementally of Elbaite. Only STEWS and STEWGMII have slightly different elemental composition variations closer to schorl than elbaite.

The results of x-ray diffractometry experimentation indicated a relationship between lattice parameters and Fe content. As Fe (*apfu*) increased, lattice parameter (*a*)

(Figure 1) and  $\langle c \rangle$  increased (Figure 2) as well as the  $\langle Z-O \rangle$  (Figure 3) and  $\langle X-O \rangle$  (Figure 4) bond-distances. Additionally, as the  $\langle Z-O \rangle$  bond-distance increased, so did the  $\langle X-O \rangle$  bond-distance (Figure 5). When the  $\langle X-O \rangle$  bond-distance increased, the lattice parameter ( $a$ ) increased as well (Figure 6). It was also found that as the  $\langle Z-O \rangle$  bond-distances increased, so did the lattice parameter ( $a$ ) (Figure 7).

As the Fe *apfu* increased, it would only be expected that there would be an increase lattice parameter ( $a$ ). Additionally, since the tourmaline unit cell predominantly has Al at the Y site, substituting Fe for Al at the Y site would increase the lattice parameter ( $a$ ). The atomic radius of Al is smaller than that of Fe, thus, increased substitution of Fe for Al would increase the lattice parameter ( $a$ ). Since the atomic radii of the Al is smaller than Fe or Mg, increased substitution of Fe at the Y site instead of Al would allow for an increased  $\langle X-O \rangle$  and  $\langle Z-O \rangle$  bond-distance. Increased substitutions of Fe for Y site Al in the unit cell causes the larger the  $\langle X-O \rangle$  (Figure 8) and  $\langle Z-O \rangle$  bond-distances (Figure 9) become and the larger the lattice parameter ( $a$ ).

### *Polyhedra Distortion*

Polyhedron distortions (Ertl *et al.* 2002) were calculated for the samples from the Stewart Mine and are displayed in Table 6. Distortions were calculated for the Y, Z, T and X polyhedra. Bond-length distortion ( $\Delta$ ), bond-angle distortion ( $\sigma^2$ ), bond-angle distortion (DI(Y-O)), bond-length distortion (DI(O-Y-O)) as defined in Ertl *et al.* 2002 were calculated for each polyhedron.

The Y site displayed a decrease in bond-angle distortion with increasing bond-length distortion of the X site ( $R^2=0.891$ ). Additionally, as the  $\langle Y-O \rangle$  bond-distance

decreased, the bond-length distortion of the *Y* site increased ( $R^2=0.817$ ) along with the bond-angle distortion of the *Z* site ( $R^2=0.985$ ). Ertl *et al.* 2002 found that bond-angle distortion was negatively correlated with  $\langle Y-O \rangle$  bond-distance however in samples from the Stewart Mine, no relationship was found and in fact bond-length distortion of the *Y* site increased as the  $\langle Y-O \rangle$  bond-distance decreased. Increasing amounts of Fe at the *Y* site decrease the bond-angle distortion ( $R^2=0.818$ ) indicating that the structure of tourmalines from the Stewart Mine became less distorted with increasing Fe content.

As the Al *Y* site *apfu* increases, the  $\langle Z-O \rangle$  bond-distance decreased ( $R^2=0.911$ ). This decrease in  $\langle Z-O \rangle$  bond-distance corresponds to an increase in Li ( $R^2=0.84$ ) and a decrease in Fe ( $R^2=0.939$ ). Additionally, the decrease in  $\langle Z-O \rangle$  bond-distance increases the *X* site bond-length distortion ( $R^2=0.891$ ) but decreases the  $\langle X-O \rangle$  bond-distance ( $R^2=0.95$ ). Decreasing  $\langle Z-O \rangle$  bond-distance increases the *T* site bond-angle distortion ( $R^2=0.829$ ). Thus, the increase in *Y* site Al causes distortions in the *Z* sites giving rise to increasing distortions in the *X* and *T* sites.

As the *Z* site bond-angles decrease, the  $\langle Y-O \rangle$  distance increases ( $R^2=0.985$ ) as well as the *Y* site bond-lengths ( $R^2=0.817$ ). This relationship from the Stewart Mine was also found in tourmaline samples from Ertl *et al.* 2002. The decrease in *Z* site bond-angles increases the *Z* site bond-lengths ( $R^2=0.873$ ) but as the *Z* site bond-length increases the  $\langle Y-O \rangle$  distance increases ( $R^2=0.936$ ) along with the *Y* site bond-length distortion ( $R^2=0.825$ ). These results indicate that changes lengths and distorts of the bond-lengths and angles of the *Y* and *Z* sites are interrelated, a conclusion substantiated by the fact that the *X* and *T* sites are connected octahedra and share edges across the O3 and O6 oxygens.

As Al *apfu* at the *Y* site increases the bond-angle distortion of the *T* site increases ( $R^2=0.757$ ), indicating that the *T* site becomes more distorted with increasing *Y* site Al. As the *T* site bond-angle distortion increases, the bond-length distortion increases ( $R^2=0.749$ ). Thus increasing *Y* site Al increases bond-length and bond-angle distortions in the *T* site.

Decreasing the  $\langle X-O \rangle$  bond-distance has a significant effect of chemistry. Decreasing the  $\langle X-O \rangle$  bond-distance causes an increase *Y* site Al ( $R^2=0.89$ ) and increase Li ( $R^2=0.871$ ) as well as a decrease in Fe ( $R^2=0.95$ ), OH ( $R^2=0.755$ ) and *X* site vacancy ( $R^2=0.746$ ). Additionally, decreasing the  $\langle X-O \rangle$  bond-distance causes an increase in *T* site bond-angle distortion ( $R^2=0.951$ ) and *X* site bond-length distortions ( $R^2=0.876$ ). *X* site bond-length distortions cause an increase in *T* site bond-angle distortion ( $R^2=0.845$ ). As evident above, in samples from the Stewart Mine, a relationship between *T* site bond-angle distortion and *X* site charge exists, in our samples this relates to the *X* site vacancy. This relationship was noted in Ertl *et al.* 2002.

Increases in *X* site bond-length distortions cause an increase in *Y* site Al ( $R^2=0.761$ ) and *X* site Na ( $R^2=0.903$ ). Conversely, decreases in *X* site bond-length distortions cause increases in Fe ( $R^2=0.88$ ) and *X* site vacancy ( $R^2=0.856$ ). Thus, increased Al and Na in the *X* and *Y* sites cause increased distortions in *X* site bond-lengths that decrease the Fe content and *X* site vacancies.

### *Mn Content*

Samples analyzed displayed a higher amount of Mn than was expected and virtually no Mg despite several of the the samples being modeled with Mg. Mn content

ranged from 0.18 to 0.52 *apfu*. Mg was present in one sample, STEWS at 0.04 *apfu*. Tourmaline analyzed from the Himalaya mine, Mesa Grande, California contained between 0.01 and 0.80 *apfu* Mn across all seven samples and 0.08 *apfu* Mg content in one sample, HMGC1 (Ertl *et al.*, 2010). The Himalaya mine produced several Mn rich yellow tourmalines containing between 0.698 and 0.944 Mn *apfu* (Simmons *et al.*, 2011). Mn rich tourmaline analyzed from Austria displays a similar trend to the Himalaya and the Stewart Mine. Samples from Eibenstein der Thaya, Lower Austria were analyzed and showed no Mg (0.00 *apfu* in all samples) and a high amount of Mn, between 1.14 and 1.23 Mn *apfu* (Ertl *et al.*, 2003).

The Mn end member of the tourmaline super group, the new mineral, Tsilaisite, can theoretically contain up to 3.0 *apfu* Mn at the *Y* site in its structural formula. However, when analyzed, Tsilaisite was only found to contain 1.34 Mn *apfu* (Bosi *et al.*, 2012). While this is significantly less than the 0.18 to 0.52 Mn *apfu* in the samples analyzed from this study, worldwide, Mn rich yellow tourmaline varies in Mn content from 0.569 to 1.078 *apfu* (Simmons *et al.*, 2011). Mg content in Mn rich yellow tourmalines is virtually nonexistent while Mg rich tourmalines can contain Mn. Mg content in the previously mentioned Mn rich tourmalines ranged from below detection limits to 0.003 Mn *apfu* (Simmons *et al.*, 2011). This could indicate that yellow Mn-rich tourmaline does not incorporate Mg into its crystal structure and chemistry. Samples from the Stewart mine followed the trend of Mn tourmaline in that it contained moderate amounts of Mn and none to virtually little amounts of Mg. Significant investigation will be required to understand the relationship between Mn and Mg tourmaline.

## ACKNOWLEDGEMENTS

This research is funded by the National Science Foundation grant NSF-MRI 1039436 awarded to JMH.

## REFERENCES

- BOSI, F. & LUCCHESI, S. (2007): Crystal chemical relationships in the tourmaline group: Structural constraints on chemical variability. *American Mineralogist* **92**, 1054-1063.
- BOSI, F., SKOGBY, H., AGROSÌ, G. & SCANDALE, E. (2012): Tsilaisite,  $\text{NaMn}_3\text{Al}_6(\text{Si}_6\text{O}_{18})(\text{BO}_3)_3(\text{OH})_3\text{OH}$ , a new mineral species of the tourmaline supergroup from Grotta d'Oggi, San Pietro in Campo, island of Elba, Italy. *American Mineralogist* **97**, 989-994.
- ERTL, A., HUGHES, J.M., PERTLICK, F., FOIT, F.F., WRIGHT, S.E., BRANDSTATTER, F. & MARLER, B. (2002): Polyhedron distortions in tourmaline. *Canadian Mineralogist* **40**, 153-162.
- ERTL, A., HUGHES, J.M., PROWATKE, S., ROSSMAN, G.R., LONDON, D. & FRITZ, E.A. (2003): Mn-rich tourmaline from Austria: structure, chemistry, optical spectra, and relations to synthetic solid solutions. *American Mineralogist* **88**, 1369-1376.
- ERTL, A., ROSSMAN, G.R., HUGHES, J.M., LONDON, D., WANG, Y., O'LEARY, J.A., DARBY, M.D., PROWATKE, S., LUDWIG, T. & TILLMANN, E. (2010): Tourmaline of the elbaite-schorl series from the Himalaya Mine, Mesa Grande, California: a detailed investigation. *American Mineralogist* **95**, 24-40.
- HAWTHORNE, F.C. (2002): Bond-valence constraints on the chemical composition of tourmaline. *Canadian Mineralogist* **40**, 789-797.
- HAWTHORNE, F.C. & HENRY, D.J. (1999): Classification of minerals of the tourmaline group. *European Journal of Mineralogy* **11**, 201-215.

- Henry, D.J., Novák, M., Hawthorne, F.C., Ertl, A., Uher, P., Dutrow, B.L., Pezzotta, F. (2011): Nomenclature of the tourmaline-group minerals. *American Mineralogist* **96**, 895-913.
- HERZOG, L.F., PINSON, W.H., JR. & HURLEY, P.M. (1960): Rb-Sr analysis and age determinations of certain lepidolites, including an international interlaboratory comparison suite. *American Journal of Science* **258**, 191-208.
- JAHNS, R.H. & WRIGHT, L.A. (1951): Gem- and lithium bearing pegmatites of the Pala District, San Diego County, California. *California Division of Mines Special Report 7-A*. 98p
- LONDON, D. (1986): Formation of tourmaline-rich gem pockets in miarolitic pegmatites. *American Mineralogist* **71**, 396-405.
- MARSCHALL, H.R. & JIANG, S.Y. (2011): Tourmaline isotopes: no element left behind. *Elements* **7**, 313-319.
- SHELDRIK, G.M. (2008): A short history of *SHELX*. *Acta Crystallogr.* **A64**, 112-122.
- SIMMONS, W.B., FALSTER, A.U. & LAURS, B.M. (2011): A survey of Mn-rich yellow tourmaline from worldwide localities and implications for the petrogenesis of granitic pegmatites. *Canadian Mineralogist* **49**, 301-319.
- TAYLOR, B.E., FOORD, E.E. & FRIEDRICHSSEN, H. (1979): Stable isotope and fluid inclusion studies of gem-bearing granitic pegmatite-aplite dikes, San Diego Co., California. *Contributions to Mineralogy and Petrology* **68**, 187-205.

TABLE 1. DATA COLLECTION AND STRUCTURAL REFINEMENT DETAILS  
 FOR TOURMALINES FROM THE STEWART MINE, PALA, SAN DIEGO  
 COUNTY, CALIFORNIA

Space group:	<i>R3m</i>		
Frame width:	0.20°		
Number of frames, detector distance:	4500, 5 cm		
Refined parameters:	94		
Unit-cell parameter (Å):			
	<i>a</i>	<i>c</i>	
STEWCL	15.8892(4)	7.1198(2)	
STEWCO	15.8669(3)	7.11250(10)	
STEWLGII	15.8657(3)	7.1107(2)	
STEWMCIII	15.8560(3)	7.10660(10)	
STEWMGII	15.9289(8)	7.1273(3)	
STEWMP	15.8556(4)	7.1038(2)	
STEWS	15.9700(3)	7.14310(10)	
Unique reflections; measured reflections:			
STEWCL	1111	10052	
STEWCO	1109	10076	
STEWLGII	1108	9952	
STEWMCIII	1108	9899	
STEWMGII	1119	10118	
STEWMP	1109	9831	
STEWS	1126	10165	
<i>R</i> <sub>1</sub> , all data; difference peaks (+,-), goodness-of-fit:			
STEWCL	0.0165	0.978, 0.249	1.08
STEWCO	0.0141	0.681, 0.278	1.145
STEWLGII	0.0137	0.684, 0.203	1.15
STEWMCIII	0.0133	0.47, 0.229	1.146
STEWMGII	0.014	0.597, 0.264	1.086
STEWMP	0.014	0.568, 0.23	1.147
STEWS	0.0119	0.478, 0.288	1.154

TABLE 2. ATOMIC COORDINATES AND EQUIVALENT ISOTROPIC ATOMIC DISPLACEMENT PARAMETERS ( $\text{\AA}^2$ ) FOR TOURMALINES FROM THE STEWART MINE, PALA, SAN DIEGO COUNTY, CALIFORNIA.

Atom	Sample	$X$	$y$	$z$	$U_{eq}$
$X$	STEWCL	0	0	1/4	0.0221(7)
	STEWCO	0	0	3/4	0.0242(7)
	STEWLGII	0	0	1/4	0.0254(7)
	STEWMCIII	0	0	3/4	0.0256(7)
	STEWMGII	0	0	1/4	0.0283(8)
	STEWMP	0	0	3/4	0.0224(7)
	STEWS	0	0	3/4	0.0256(11)
$T$	STEWCL	0.19193(3)	0.18994(3)	0.0155(3)	0.00579(10)
	STEWCO	0.80808(2)	0.81010(2)	0.9838(3)	0.00563(9)
	STEWLGII	0.19191(2)	0.18987(2)	0.0166(3)	0.00570(9)
	STEWMCIII	0.80816(2)	0.81019(2)	0.9820(3)	0.00555(9)
	STEWMGII	0.19194(2)	0.18995(2)	0.0178(3)	0.00664(10)
	STEWMP	0.80807(2)	0.81014(2)	0.9831(3)	0.00591(9)
	STEWS	0.80811(2)	0.81007(2)	0.9726(4)	0.00553(9)
$B$	STEWCL	0.10943(8)	0.21886(17)	0.4701(4)	0.0073(4)
	STEWCO	0.89077(7)	0.78153(14)	0.5291(4)	0.0070(3)
	STEWLGII	0.10924(7)	0.21848(14)	0.4709(4)	0.0071(3)
	STEWMCIII	0.89072(6)	0.78144(12)	0.5283(4)	0.0071(3)
	STEWMGII	0.10977(7)	0.21953(15)	0.4722(4)	0.0085(3)
	STEWMP	0.89089(7)	0.78179(15)	0.5293(4)	0.0074(3)
	STEWS	0.88983(7)	0.77965(14)	0.5186(5)	0.0077(3)
${}^Y\text{Al}$	STEWCL	0.12364(6)	0.06182(3)	0.6441(3)	0.0102(2)
	STEWCO	0.87679(5)	0.93839(3)	0.3529(3)	0.0094(2)
	STEWLGII	0.12315(5)	0.06157(2)	0.6477(3)	0.0092(2)
	STEWMCIII	0.87785(4)	0.93892(2)	0.3497(3)	0.0095(2)
	STEWMGII	-	-	-	-
	STEWMP	0.87683(6)	0.93842(3)	0.3507(3)	0.0085(3)
	STEWS	-	-	-	-
${}^Y\text{Li}$	STEWCL	0.12364(6)	0.06182(3)	0.6441(3)	0.0102(2)
	STEWCO	0.87679(5)	0.93839(3)	0.3529(3)	0.0094(2)
	STEWLGII	0.12315(5)	0.06157(2)	0.6477(3)	0.0092(2)
	STEWMCIII	-	-	-	-
	STEWMGII	-	-	-	-

	STEWMP	0.87683(6)	0.93842(3)	0.3507(3)	0.0085(3)
	STEWS	-	-	-	-
<sup>Y</sup> Mg	STEWCL	-	-	-	-
	STEWCO	-	-	-	-
	STEWLGII	-	-	-	-
	STEWMCIH	-	-	-	-
	STEWMGII	0.12343(3)	0.061717(16)	0.6453(4)	0.00947(16)
	STEWMP	-	-	-	-
	STEWS	0.87658(2)	0.938288(11)	0.3447(4)	0.00880(11)
<sup>Y</sup> Fe	STEWCL	-	-	-	-
	STEWCO	-	-	-	-
	STEWLGII	-	-	-	-
	STEWMCIH	-	-	-	-
	STEWMGII	0.12343(3)	0.061717(16)	0.6453(4)	0.00947(16)
	STEWMP	-	-	-	-
	STEWS	0.87658(2)	0.938288(11)	0.3447(4)	0.00880(11)
<sup>Z</sup> Al	STEWCL	0.29734(3)	0.26057(3)	0.6266(3)	0.00670(13)
	STEWCO	0.70294(3)	0.73974(3)	0.3732(3)	0.00661(11)
	STEWLGII	0.29707(3)	0.26033(3)	0.6267(3)	0.00665(11)
	STEWMCIH	0.70313(2)	0.73980(2)	0.3729(3)	0.00653(11)
	STEWMGII	0.29778(3)	0.26104(3)	0.6284(4)	0.00761(12)
	STEWMP	0.70314(3)	0.73983(3)	0.3735(3)	0.00655(12)
	STEWS	0.70180(2)	0.73865(2)	0.3628(4)	0.00634(11)
O1	STEWCL	0	0	0.7978(5)	0.0414(10)
	STEWCO	0	0	0.2013(5)	0.0352(7)
	STEWLGII	0	0	0.7973(5)	0.0339(7)
	STEWMCIH	0	0	0.2043(4)	0.0279(6)
	STEWMGII	0	0	0.7988(5)	0.0392(8)
	STEWMP	0	0	0.2034(5)	0.0295(7)
	STEWS	0	0	0.1927(5)	0.0319(7)
O2	STEWCL	0.06061(6)	0.12123(12)	0.4994(4)	0.0188(4)
	STEWCO	0.93946(5)	0.87893(10)	0.4974(4)	0.0172(3)
	STEWLGII	0.06054(5)	0.12107(10)	0.5036(4)	0.0166(3)
	STEWMCIH	0.93942(5)	0.87885(9)	0.4941(4)	0.0158(3)
	STEWMGII	0.06131(5)	0.12262(10)	0.5028(4)	0.0192(3)
	STEWMP	0.93959(5)	0.87917(11)	0.4956(4)	0.0164(3)
	STEWS	0.93819(5)	0.87638(9)	0.4860(5)	0.0165(3)
O3	STEWCL	0.26766(14)	0.13383(7)	0.5246(4)	0.0124(3)
	STEWCO	0.73344(12)	0.86672(6)	0.4751(4)	0.0126(3)
	STEWLGII	0.26594(11)	0.13297(6)	0.5248(4)	0.0128(3)
	STEWMCIH	0.73575(11)	0.86788(5)	0.4743(4)	0.0131(2)
	STEWMGII	0.26766(11)	0.13383(6)	0.5267(4)	0.0127(3)
	STEWMP	0.73500(12)	0.86750(6)	0.4762(4)	0.0132(3)

O4	STEWS	0.73251(10)	0.86626(5)	0.4636(5)	0.0124(2)
	STEWCL	0.09324(6)	0.18648(12)	0.0876(3)	0.0095(3)
	STEWCO	0.90653(5)	0.81306(10)	0.9116(3)	0.0093(2)
	STEWLGII	0.09359(5)	0.18717(10)	0.0888(3)	0.0096(2)
	STEWMCIH	0.90604(5)	0.81209(9)	0.9093(3)	0.0096(2)
	STEWMGII	0.09356(5)	0.18712(10)	0.0882(4)	0.0105(2)
	STEWMP	0.90629(5)	0.81259(10)	0.9102(3)	0.0101(2)
O5	STEWS	0.90637(5)	0.81274(9)	0.9041(5)	0.0102(2)
	STEWCL	0.18658(12)	0.09329(6)	0.1097(3)	0.0098(3)
	STEWCO	0.81289(10)	0.90645(5)	0.8892(3)	0.0096(2)
	STEWLGII	0.18725(10)	0.09362(5)	0.1115(3)	0.0098(2)
	STEWMCIH	0.81251(9)	0.90625(5)	0.8869(3)	0.0099(2)
	STEWMGII	0.19728(7)	0.18691(7)	0.7927(4)	0.00982(18)
	STEWMP	0.81263(11)	0.90632(5)	0.8876(4)	0.0103(2)
O6	STEWS	0.81216(10)	0.90608(5)	0.8814(4)	0.0103(2)
	STEWCL	0.19657(8)	0.18643(8)	0.7908(3)	0.0091(2)
	STEWCO	0.80385(6)	0.81416(6)	0.2088(3)	0.00883(17)
	STEWLGII	0.19605(6)	0.18563(6)	0.7912(3)	0.00878(17)
	STEWMCIH	0.80449(6)	0.81497(6)	0.2078(3)	0.00863(16)
	STEWMGII	0.19728(7)	0.18691(7)	0.7927(4)	0.00982(18)
	STEWMP	0.80443(7)	0.81489(7)	0.2088(3)	0.00879(18)
O7	STEWS	0.80232(6)	0.81266(6)	0.1976(5)	0.00884(17)
	STEWCL	0.28593(7)	0.28586(7)	0.0955(3)	0.00758(19)
	STEWCO	0.71392(6)	0.71408(6)	0.9044(3)	0.00743(16)
	STEWLGII	0.28620(6)	0.28603(6)	0.0956(3)	0.00737(16)
	STEWMCIH	0.71357(6)	0.71379(5)	0.9039(3)	0.00730(15)
	STEWMGII	0.28569(6)	0.28599(6)	0.0973(4)	0.00877(17)
	STEWMP	0.71357(6)	0.71380(6)	0.9046(3)	0.00763(17)
O8	STEWS	0.71470(6)	0.71410(6)	0.8939(4)	0.00815(16)
	STEWCL	0.20987(8)	0.27052(8)	0.4563(3)	0.0089(2)
	STEWCO	0.79027(7)	0.72967(7)	0.5436(3)	0.00883(18)
	STEWLGII	0.20968(6)	0.27034(7)	0.4562(3)	0.00863(18)
	STEWMCIH	0.79032(6)	0.72955(6)	0.5432(3)	0.00845(16)
	STEWMGII	0.20999(7)	0.27074(7)	0.4582(4)	0.01008(19)
	STEWMP	0.79049(7)	0.72992(7)	0.5441(3)	0.00856(18)
	STEWS	0.79000(6)	0.72913(7)	0.5326(4)	0.00963(17)

TABLE 3. SELECTED BOND-DISTANCES (Å) FOR TOURMALINES FROM THE  
STEWART MINE, PALA, SAN DIEGO COUNTY, CALIFORNIA

	STEWCL	STEWCO	STEWLGII	STEWMCIII	STEWMGII	STEWMP	STEWS
<i>X-</i>							
O(2) (x3)	2.4360(2)	2.4490(2)	2.4530(2)	2.4650(2)	2.4710(2)	2.4530(2)	2.5450(3)
O(5) (x3)	2.7551(17)	2.7552(15)	2.7549(15)	2.7522(15)	2.7694(17)	2.7522(17)	2.7623(17)
O(4) (x3)	2.8146(18)	2.8142(16)	2.8155(15)	2.8177(15)	2.8272(17)	2.8137(17)	2.8140(17)
Mean:	2.6686	2.6728	2.6745	2.6783	2.6892	2.6730	2.7071
<i>Y-</i>							
O(2) (x2)	1.9750(12)	1.9681(10)	1.9661(10)	1.9607(9)	1.9778(10)	1.9665(11)	1.9844(9)
O(6) (x2)	2.0149(12)	1.9986(10)	1.9944(10)	1.9865(9)	2.0296(10)	1.9802(11)	2.0385(9)
O(1)	2.023(2)	2.0071(17)	1.9988(16)	1.9700(15)	2.0240(17)	1.9885(18)	2.0227(15)
O(3)	2.1567(19)	2.1531(17)	2.1478(16)	2.1428(15)	2.1617(16)	2.1420(18)	2.1660(15)
Mean:	2.0424	2.0317	2.0268	2.015	2.0483	2.0193	2.0529
<i>Z-</i>							
O(6)	1.8524(12)	1.8535(10)	1.8555(9)	1.8613(9)	1.8543(10)	1.8583(10)	1.8622(9)
O(7)	1.8831(11)	1.8840(9)	1.8826(9)	1.8822(8)	1.8792(9)	1.8821(10)	1.8789(9)
O(8)	1.88(11)	1.8847(10)	1.8845(9)	1.8846(9)	1.8822(10)	1.8872(10)	1.8836(9)
O(8')	1.9100(11)	1.9066(9)	1.9070(9)	1.9048(9)	1.9149(10)	1.9049(10)	1.9218(9)
O(7')	1.9526(11)	1.9516(9)	1.9489(9)	1.9461(8)	1.9540(10)	1.9462(9)	1.9603(9)
O(3)	1.9637(8)	1.9606(7)	1.9633(7)	1.9648(6)	1.9724(7)	1.9655(7)	1.9782(7)
Mean:	1.9070	1.9068	1.9070	1.9073	1.9095	1.9074	1.9142
<i>T-</i>							
O(6)	1.6038(11)	1.6043(10)	1.6063(10)	1.6085(9)	1.6085(10)	1.6072(10)	1.6115(9)
O(7)	1.6131(10)	1.6112(8)	1.6121(8)	1.6128(8)	1.6145(9)	1.6128(9)	1.6139(9)
O(4)	1.6245(6)	1.6225(5)	1.6226(5)	1.6219(5)	1.6243(5)	1.6234(6)	1.6240(5)
O(5)	1.6385(7)	1.6366(6)	1.6370(6)	1.6363(6)	1.6374(6)	1.6373(6)	1.6373(6)
Mean:	1.6200	1.6187	1.6195	1.6199	1.6212	1.6202	1.6217
<i>B-</i>							
O(2)	1.360(3)	1.357(2)	1.358(2)	1.359(2)	1.355(2)	1.358(2)	1.358(2)
O(8) (x2)	1.3857(16)	1.3851(13)	1.3842(13)	1.3830(12)	1.3862(14)	1.3829(14)	1.3843(13)
Mean:	1.3729	1.3711	1.3711	1.371	1.3706	1.3705	1.3712

TABLE 4. COMPOSITIONS OF TOURMALINES FROM THE STEWART MINE,  
PALA, SAN DIEGO, CALIFORNIA

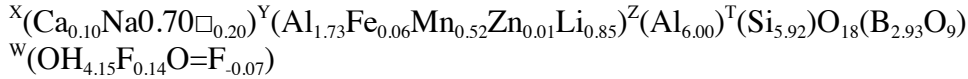
	STEWCL	STEWCO	STEWLG	STEWMC	STEWMGII	STEWMP	STEWS
SiO <sub>2</sub> wt %	36.08	37.26	36.48	36.49	35.27	36.09	34.08
TiO <sub>2</sub>	-	-	0.03	-	0.04	-	0.06
Al <sub>2</sub> O <sub>3</sub>	40.01	40.90	41.57	43.10	38.30	43.01	35.54
B <sub>2</sub> O <sub>3</sub>	10.36	10.93	10.93	11.07	10.35	11.18	10.33
FeO	0.47	0.88	1.54	0.14	4.92	-	13.45
MnO	3.75	1.91	1.35	2.12	2.72	1.47	0.76
MgO	-	-	-	-	-	-	0.16
ZnO	0.11	0.09	0.13	0.21	1.69	-	0.48
CaO	0.55	0.22	0.14	0.06	-	0.44	0.00
Na <sub>2</sub> O	2.21	2.13	2.17	2.05	2.14	1.88	1.44
Li <sub>2</sub> O	1.28	1.49	1.39	1.16	0.63	1.49	0.06
H <sub>2</sub> O	3.09	3.34	3.34	3.59	3.64	3.51	3.70
F	1.54	1.13	1.12	0.79	0.83	1.17	0.26
O=F	-0.65	-0.48	-0.47	-0.33	-0.35	-0.49	-0.11
Sum	98.16	99.33	99.26	100.11	99.82	99.25	100.10
<i>N</i> anions	31	31	31	31	31	31	31
Si <i>apfu</i>	5.92	5.76	5.84	5.96	5.81	5.73	5.74
B	0.00	0.02	0.00	-	0.00	0.06	-
Al	-	-	-	0.04	-	-	0.26
Sum <i>T</i> site	5.92	5.78	5.84	6.00	5.81	5.79	6.00
B	2.93	3.00	3.00	3.01	2.96	3.00	3.00
Al	7.73	8.02	7.85	7.70	7.43	8.04	6.79
Fe	0.06	0.02	0.21	0.12	0.68	-	1.89
Mn	0.52	0.28	0.18	0.26	0.38	0.20	0.11
Mg	-	-	-	-	-	-	0.04
Li	0.85	0.73	0.90	0.96	0.42	0.95	0.04
Zn	0.01	0.02	0.20	0.01	0.21	-	0.06
Ti	-	-	-	-	-	-	0.01
Sum <i>Y,Z</i> site	9.17	9.07	9.34	9.05	9.12	9.19	8.94
Ca	0.10	0.01	0.02	0.04	-	0.04	-
Na	0.70	0.63	0.67	0.66	0.68	0.66	0.47
K	-	-	-	-	-	-	-
□	0.20	0.36	0.31	0.30	0.32	0.30	0.53
Sum <i>X</i> site	1.00	1.00	1.00	1.00	1.00	1.00	1.00

Sum cations	16.17	16.07	16.34	16.05	16.12	16.19	15.94
OH	3.38	3.79	3.57	3.56	4.00	3.71	4.15
F	0.80	0.39	0.57	0.57	0.43	0.59	0.14
O=F	-0.40	-0.20	-0.28	-0.29	-0.22	-0.29	-0.07
Sum OH+F+O=F	3.78	3.98	3.86	3.84	4.21	4.01	4.22

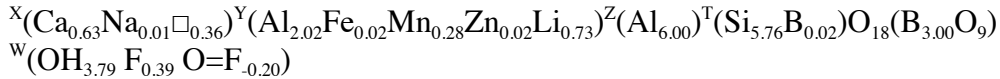
---

TABLE 5. MINERAL FORMULAS FOR TOURMALINES FROM THE STEWART  
MINE, PALA, SAN DIEGO COUNTY, CALIFORNIA

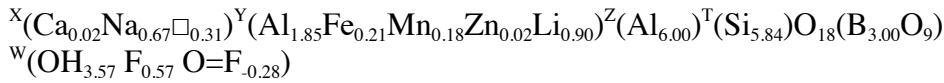
**STEWCL:**



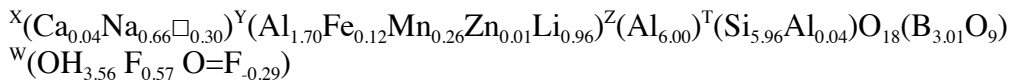
**STEWCO:**



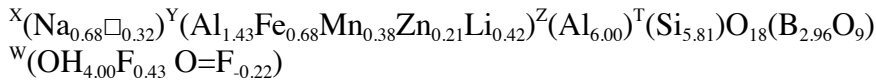
**STEWLGII:**



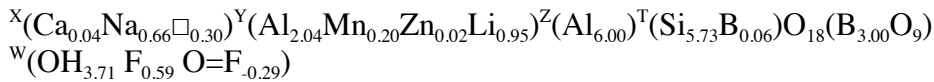
**STEWMCIII:**



**STEWMGII:**



**STEWMP:**



**STEW S:**

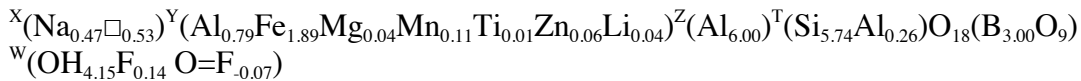


TABLE 6: POLYHEDRON DISTORTIONS IN TOURMALINES FROM THE STEWART MINE, PALA, SAN DIEGO COUNTY, CALIFORNIA

Y-	<i>a</i> [Å]	<i>c</i> [Å]	Y Site (main elements)	$\Delta_{\text{oct}}$ $\times 10^3$	$\sigma_{\text{oct}}^2$	DI (Y-O)	DI (O-Y-O)	<Y-O> [Å]
AESTEWC	15.8892(4)	7.1198(2)	Al <sub>1.73</sub> Fe <sub>0.06</sub> Mn <sub>0.52</sub> Zn <sub>0.01</sub> Li <sub>0.85</sub>	0.96	80.8	0.026	0.080	2.0424
AESTEWC	15.8669(3)	7.11250(10)	Al <sub>2.02</sub> Fe <sub>0.02</sub> Mn <sub>0.28</sub> Zn <sub>0.02</sub> Li <sub>0.73</sub>	1.03	80.2	0.028	0.080	2.0317
AESTEWLGII	15.8657(3)	7.1107(2)	Al <sub>1.85</sub> Fe <sub>0.21</sub> Mn <sub>0.18</sub> Zn <sub>0.02</sub> Li <sub>0.90</sub>	1.01	53.0	0.028	0.081	2.0268
AESTEWMCI	15.8560(3)	7.10660(10)	Al <sub>1.70</sub> Fe <sub>0.12</sub> Mn <sub>0.26</sub> Zn <sub>0.01</sub> Li <sub>0.96</sub>	1.07	81.7	0.028	0.082	2.0150
AESTEWMGII	15.9289(8)	7.1273(3)	Al <sub>1.43</sub> Fe <sub>0.68</sub> Mn <sub>0.38</sub> Zn <sub>0.21</sub> Li <sub>0.42</sub>	0.96	85.3	0.026	0.084	2.0483
AESTEWMP	15.8556(4)	7.1038(2)	Al <sub>2.04</sub> Mn <sub>0.20</sub> Zn <sub>0.02</sub> Li <sub>0.95</sub>	1.01	78.9	0.028	0.080	2.0193
AESTEWS	15.9700(3)	7.14310(10)	Al <sub>0.79</sub> Fe <sub>1.89</sub> Mg <sub>0.04</sub> Mn <sub>0.11</sub> Ti <sub>0.01</sub> Zn <sub>0.06</sub> Li <sub>0.04</sub>	0.93	88.1	0.025	0.086	2.0529

Z-	<i>a</i> [Å]	<i>c</i> [Å]	Z Site (main elements)	$\Delta_{\text{oct}}$ $\times 10^3$	$\sigma_{\text{oct}}^2$	DI (Z-O)	DI (O-Z-O)	<Z-O> [Å]
AESTEWC	15.8892(4)	7.1198(2)	Al <sub>6.00</sub>	0.44	46.7	0.018	0.059	1.907
AESTEWC	15.8669(3)	7.11250(10)	Al <sub>6.00</sub>	0.40	48.1	0.017	0.06	1.907
AESTEWLGII	15.8657(3)	7.1107(2)	Al <sub>6.00</sub>	0.40	48.7	0.017	0.061	1.907
AESTEWMCI	15.8560(3)	7.10660(10)	Al <sub>6.00</sub>	0.37	50.8	0.017	0.062	1.907
AESTEWMGII	15.9289(8)	7.1273(3)	Al <sub>6.00</sub>	0.49	46.3	0.020	0.059	1.910
AESTEWMP	15.8556(4)	7.1038(2)	Al <sub>6.00</sub>	0.38	49.8	0.017	0.062	1.907
AESTEWS	15.9700(3)	7.14310(10)	Al <sub>6.00</sub>	0.51	45.7	0.021	0.058	1.914

T-	<i>a</i> [Å]	<i>c</i> [Å]	T Site (main elements)	$\Delta_{\text{tet}}$ $\times 10^3$	$\sigma_{\text{tet}}^2$	DI (T-O)	DI (O-T-O)
AESTEWC	15.8892(4)	7.1198(2)	Si <sub>5.92</sub>	0.03	7.87	0.007	0.017
AESTEWC	15.8669(3)	7.11250(10)	Si <sub>5.76</sub> B <sub>0.02</sub>	0.03	7.03	0.007	0.016
AESTEWLGII	15.8657(3)	7.1107(2)	Si <sub>5.84</sub>	0.02	6.80	0.006	0.016
AESTEWMCI	15.8560(3)	7.10660(10)	Si <sub>5.96</sub> Al <sub>0.04</sub>	0.02	6.04	0.006	0.015
AESTEWMGII	15.9289(8)	7.1273(3)	Si <sub>5.81</sub>	0.02	5.43	0.006	0.014
AESTEWMP	15.8556(4)	7.1038(2)	Si <sub>5.73</sub> B <sub>0.06</sub>	0.02	6.86	0.006	0.016
AESTEWS	15.9700(3)	7.14310(10)	Si <sub>5.74</sub> Al <sub>0.26</sub>	0.02	3.99	0.006	0.012

X-	<i>a</i> [Å]	<i>c</i> [Å]	X Site (main elements)	$\Delta_x$ $\times 10^3$	DI (X-O)	DI (O-X-O)	<X-O> [Å]
AESTEWC	15.8892(4)	7.1198(2)	Ca <sub>0.10</sub> Na <sub>0.70</sub> □ <sub>0.20</sub>	3.88	0.058	0.153	2.6686
AESTEWC	15.8669(3)	7.11250(10)	Ca <sub>0.63</sub> Na <sub>0.01</sub> □ <sub>0.36</sub>	3.59	0.056	0.151	2.6728
AESTEWLII	15.8657(3)	7.1107(2)	Ca <sub>0.02</sub> Na <sub>0.67</sub> □ <sub>0.31</sub>	3.51	0.055	0.151	2.6745
AESTEWMCIII	15.8560(3)	7.10660(10)	Ca <sub>0.04</sub> Na <sub>0.66</sub> □ <sub>0.30</sub>	3.27	0.053	0.149	2.6783
AESTEWMGII	15.9289(8)	7.1273(3)	Na <sub>0.68</sub> □ <sub>0.32</sub>	3.37	0.054	0.152	2.6892
AESTEWMP	15.8556(4)	7.1038(2)	Ca <sub>0.04</sub> Na <sub>0.66</sub> □ <sub>0.30</sub>	3.47	0.055	0.150	2.673
AESTEWS	15.9700(3)	7.14310(10)	Na <sub>0.47</sub> □ <sub>0.53</sub>	1.85	0.040	0.145	2.7071

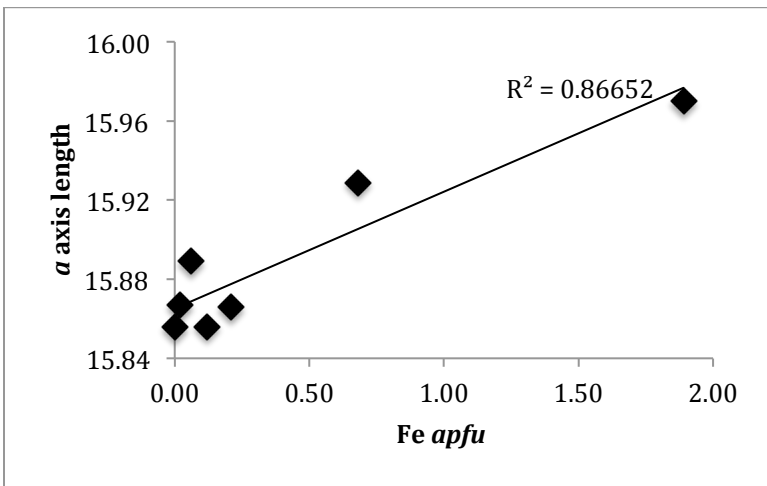


FIG. 1. Trendline showing increasing *a* axis length with increasing Fe *apfu*.

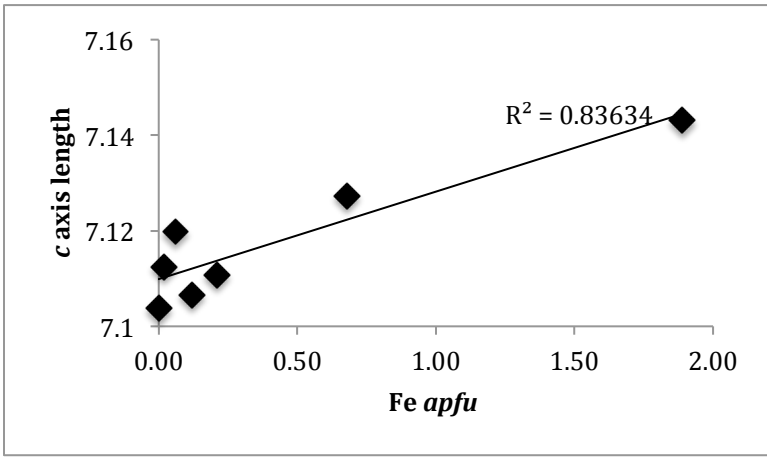


FIG. 2. Trend of increasing Fe *apfu* with increasing *c* axis length.

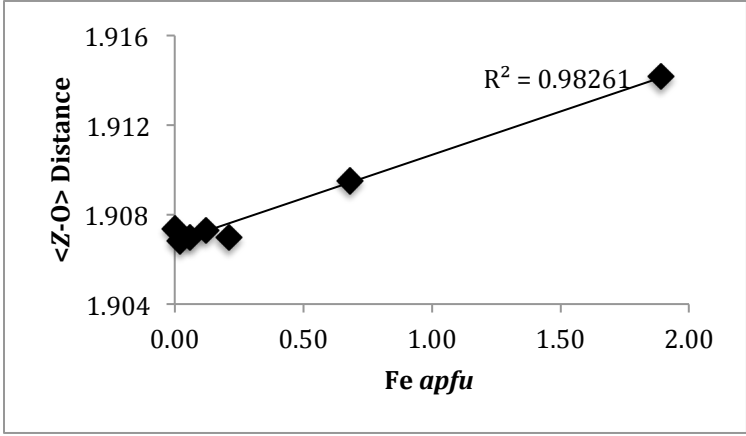


FIG. 3. Trendline displaying increasing Mean  $\langle Z-O \rangle$  bond-distance and increasing Fe *apfu*.

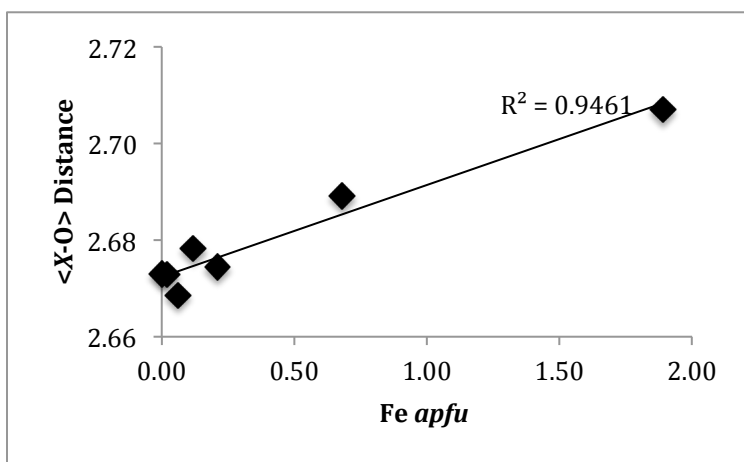


FIG. 4. Trendline displaying increasing mean  $\langle X-O \rangle$  bond-distance and increasing Fe *apfu*.

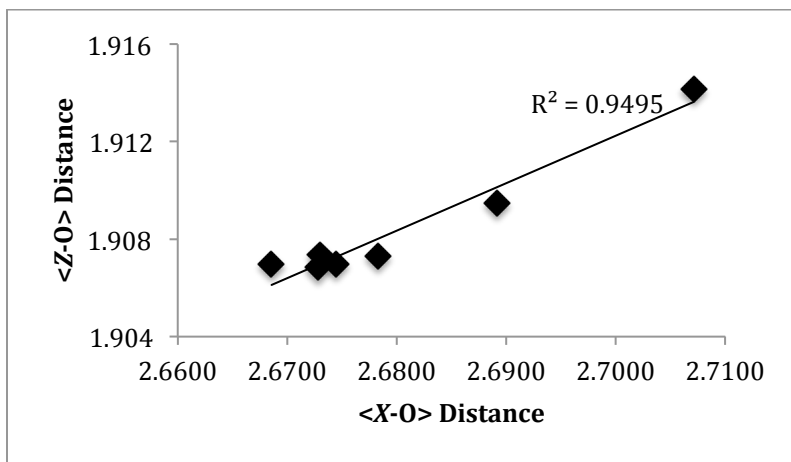


FIG. 5. Trendline displaying increasing mean  $\langle X-O \rangle$  bond-distance and increasing mean  $\langle Z-O \rangle$  bond-distance.

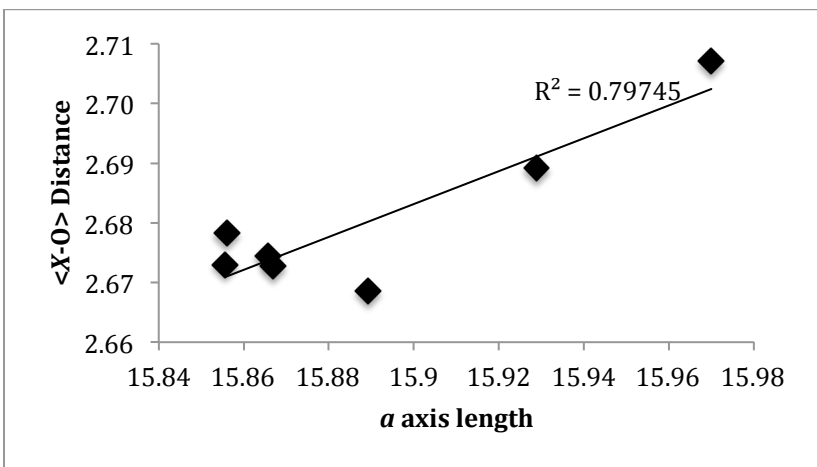


FIG. 6. Trend displaying increasing mean  $\langle X-O \rangle$  bond-distance with increasing  $a$  axis length.

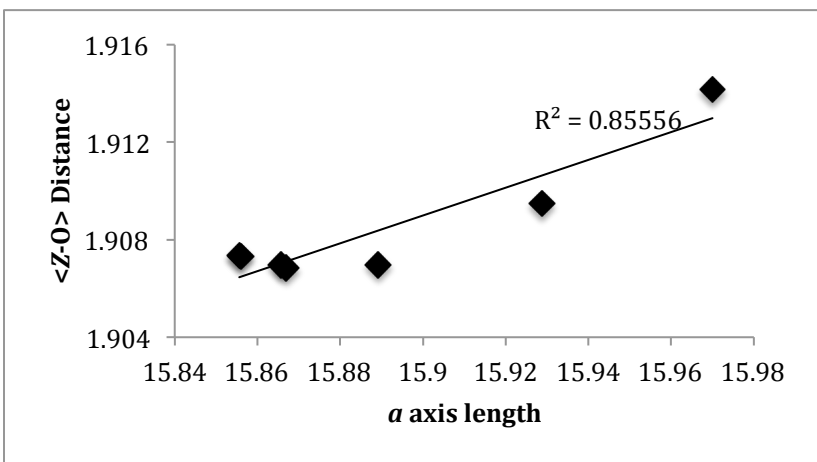


FIG. 7. Trendline illustrating relationship between increasing mean  $\langle Z-O \rangle$  bond-distance with increasing  $a$  axis length.

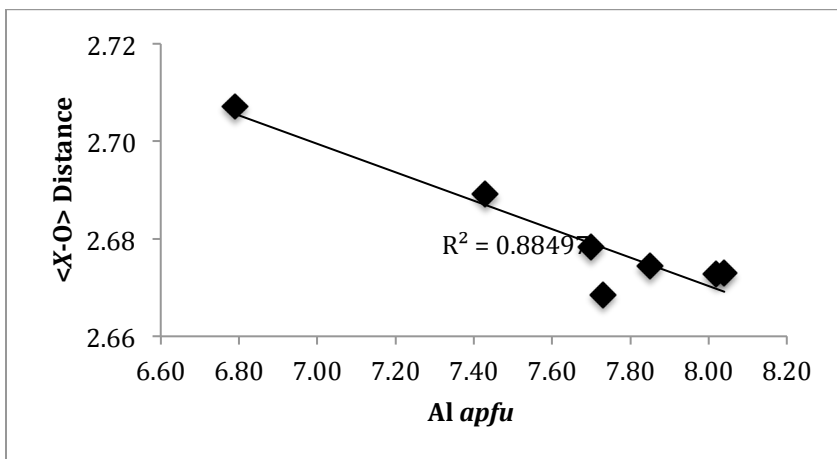


FIG. 8. Relationship between decreasing mean <X-O> bond-distance and increasing Al apfu.

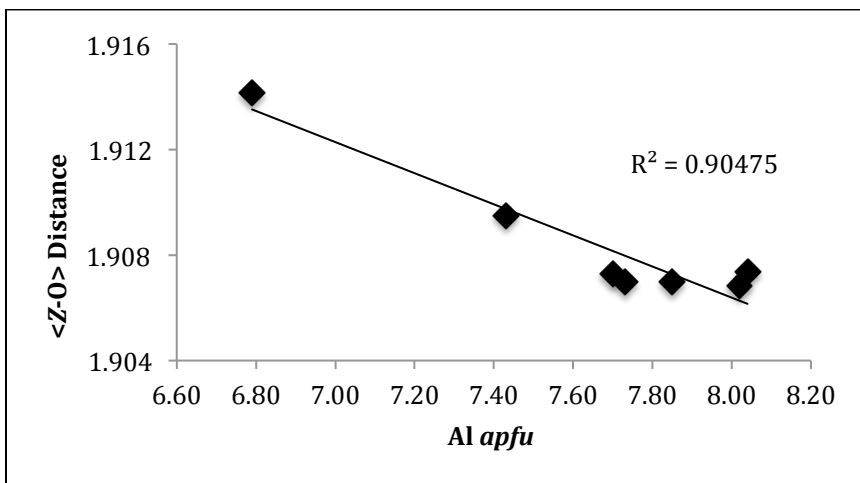


FIG. 9. Relationship between decreasing mean <Z-O> bond-distance and increasing Al apfu.